Biogeochemistry (2017) 132:165–184
DOI 10.1007/s10533-017-0294-0

Colimitation and the coupling of N and P uptake kinetics in oligotrophic mountain streams

Leslie R. Piper · Wyatt F. Cross · Brian L. McGlynn

Received: 8 July 2016 / Accepted: 7 January 2017 / Published online: 18 January 2017

Abstract Ecosystem element cycles can be tightly linked by both abiotic and biotic processes. Evidence for multi-element limitation (i.e., colimitation) of a variety of ecosystem processes is growing rapidly, yet our ability to quantify patterns of coupled nutrient dynamics at the ecosystem level has been hindered by logistical and methodological constraints. Here we quantify coupled nitrogen and phosphorus uptake kinetics in three oligotrophic mountain streams by using novel experimental techniques that quantify colimitation dynamics across a range of nutrient concentrations and stoichiometries. We show that relative demand for NO_3-N and PO_4-P varied across streams, but that short term availability of one nutrient consistently resulted in elevated, but variable, uptake of the other nutrient at all sites. We used temporally offset, pulsed nutrient additions to parameterize dual-nutrient Michaelis–Menten uptake surface models that represent NO_3-N and PO_4-P uptake at any given concentration or dissolved NO_3-N:PO_4-P stoichiometry. Our results indicated that the uptake of N and P were strongly enhanced in the presence of the other nutrient. Surface models quantitatively reflect patterns of colimitation and multi-element demand in streams, and should allow for parameterization of more realistic stream network models that explicitly account for interactions among element cycles.

Keywords Colimitation · Stream ecosystem · Ecological stoichiometry · Nitrogen and phosphorus uptake · Tracer Additions for Spiraling Curve Characterization (TASCC)

Responsible Editor: Chris D. Evans.

L. R. Piper · W. F. Cross (✉)
Department of Ecology, Montana State University, 310 Lewis Hall, Bozeman, MT 59717, USA
e-mail: wyatt.cross@montana.edu

B. L. McGlynn
Division of Earth and Ocean Sciences, Nicholas School of the Environment, Duke University, 109 Old Chemistry, Durham, NC 27708, USA

Introduction

Biogeochemical cycles of carbon (C), nitrogen (N), phosphorus (P), and other elements can be tightly linked by both abiotic and biotic processes (Melillo et al. 2003; Falkowski et al. 2008; Schlesinger et al. 2011). Biotic demand for nutrients largely results from an organisms requirements for multiple elements in relatively constrained ratios, or stoichiometries (Sterner and Elser 2002). Any shift in the availability of one element can thereby impact cycling of other elements through their shared use by organisms (Elser et al. 2009; Marklein and Houlton 2012; Appling and Heffernan 2014). Understanding linkages among elemental cycles is vital because many anthropogenic activities alter pools and fluxes of one or more

elements (Galloway et al. 2008; Finzi et al. 2011), altering the balance of available nutrients in ecosystems, the demand for these nutrients by organisms, and the pace of ecosystem processes.

There is increasing evidence in both aquatic and terrestrial ecosystems that colimitation and interactions among multiple elements may be the rule, rather than the exception (e.g., Francoeur 2001; Elser et al. 2007; Allgeier et al. 2011; Harpole et al. 2011). Indeed, hundreds of bioassays and field experiments show that primary producers respond positively to additions of both nitrogen and phosphorus across a wide diversity of ecosystem types (Elser et al. 2007), shifting the paradigm away from one of single nutrient limitation in ecosystems (e.g., Lewis and Wurtsabugh 2008; Sterner 2008; Bracken et al. 2015). Yet, most of these experiments were conducted at relatively small spatial scales, limiting their applicability towards understanding or modeling nutrient limitation at the ecosystem level. Additional research is now needed to quantify colimitation and linkages among nutrient cycles at the level of whole ecosystems that contain the full suite of habitats, microenvironments, and taxa that contribute to integrated system-level processes such as nutrient uptake and ecosystem metabolism. Streams and rivers are particularly amenable to such investigations.

Methods developed in streams to measure whole-system nutrient uptake (Stream Solute Workshop 1990) have helped bridge the gap between small-scale experiments and inference about nutrient limitation in natural ecosystems, incorporating benthic, hyporheic, and water column habitats (Mulholland and Webster 2010). These methods have been applied extensively, but most studies have focused on a single nutrient, often at ambient or near ambient nutrient concentrations (Mulholland et al. 2002; but see Dodds et al. 2002; Gibson et al. 2015). When multiple nutrients have been considered, inference has generally been derived from post hoc comparisons among separate nutrient additions (Davis and Minshall 1999; Simon et al. 2005; Johnson et al. 2009; Martí et al. 2009), or from simultaneous uptake measurements made from a single "cocktail" addition, resulting in a single set of nutrient concentrations and a single stoichiometric ratio of uptake (Johnson et al. 2009). Although the sub-field of ecological stoichiometry provides a theoretical framework for examining ecosystem-level uptake of multiple nutrients (Sterner and Elser 2002; Cross et al. 2005), the enormous amount of data and time required to test stoichiometric hypotheses has resulted in relatively little empirical work at the ecosystem scale (Brookshire et al. 2005; Schade et al. 2011; Gibson and O'Reilly 2012; Cohen et al. 2013; Rodríguez-Cardona et al. 2015).

With recent methodological developments, we can now examine whole-stream nutrient uptake kinetics quickly and efficiently (Powers et al. 2009; Covino et al. 2010a; Trentman et al. 2015). The Tracer Additions for Spiraling Curve Characterization (TASCC) method (Covino et al. 2010a, b, 2012) facilitates measurement of uptake dynamics across a range of concentrations during a single instantaneous nutrient addition. This method enables the application of previously time- and resource-prohibitive experimental approaches, and presents an opportunity for explicit examination of coupled nutrient dynamics at the ecosystem level. In particular, additions of multiple nutrients may be staggered in time, allowing one to quantify coupled nutrient uptake patterns as a function of variation in both concentration *and* stoichiometry (e.g., nitrogen to phosphorus ratios). Such an approach should enable assessment of how system-level demand for a given nutrient changes in response to the availability of other nutrients, informing our general understanding of nutrient limitation and colimitation in streams. In addition, this approach may be useful for parameterizing stream network models that aim to incorporate the dynamics of multiple elements in space and time (e.g., Helton et al. 2011).

Here, we develop and test a novel experimental approach for quantifying *coupled* nutrient dynamics in streams using the TASCC method (Covino et al. 2010a). We conducted individual and time-lagged dual N and P additions, which allowed us to quantify dual nutrient uptake kinetics across ranges of concentration and stoichiometry. These novel experimental and analytical approaches allowed us to explore three general questions: (a) are nutrient-poor mountain streams colimited by nitrogen and phosphorus?; (b) how does the availability of phosphorus influence nitrogen uptake kinetics, and vis-versa?; and (c) can dual-nutrient uptake surface models be used to advance our understanding and prediction of colimitation patterns in streams?

Methods

Study area

We studied three high-elevation streams within the West Fork of the Gallatin River watershed (212 km^2) in the northern Rocky Mountains of southwestern Montana (Fig. 1). The West Fork watershed is characterized by well-defined steep topography and shallow soils, with elevations ranging from approximately 1800 to 3400 m. Surficial geology is comprised of colluviums and glacial deposits in the valley bottoms, while higher elevations consist largely of sedimentary and metasedimentary formations of various ages as well as metamorphosed volcanic of Archean age (Gardner and McGlynn 2009; Montross et al. 2013). Average annual precipitation ranges from less than 500 mm near the watershed outlet to over 1270 mm at higher elevations, with 60% of total precipitation falling during the winter and spring months as snow (Lone Mountain NRCS Snotel #590, 2707 m elevation). The active growing season in the West Fork watershed is short, generally lasting from mid-June to mid-September. Upland vegetation is dominated by coniferous forest (Lodgepole pine, Blue and Engelmann spruce, and Douglas fir), shrubland, and native grasses, with willow and aspen groves occurring in riparian areas. For additional site information, see Gardner and McGlynn (2009).

The West Fork watershed contains four large ski resorts, including Big Sky, Moonlight Basin, Yellowstone Club, and Spanish Peaks, as well as associated residential and commercial development (Gardner and McGlynn 2009; Gardner et al. 2011; Covino et al. 2012). However, our three study reaches were chosen to represent oligotrophic streams with very little development in their sub-catchments. Beehive Creek (BH) is a second-order stream running from forested headwaters into an open meadow, with three houses and associated septic systems located within the contributing 5.7 km^2 subwatershed. Yellow Mule Creek (YM) is a first-order stream draining a 14 km^2 steep, forested catchment with our study reach located down-gradient of a small secondary gravel road. The

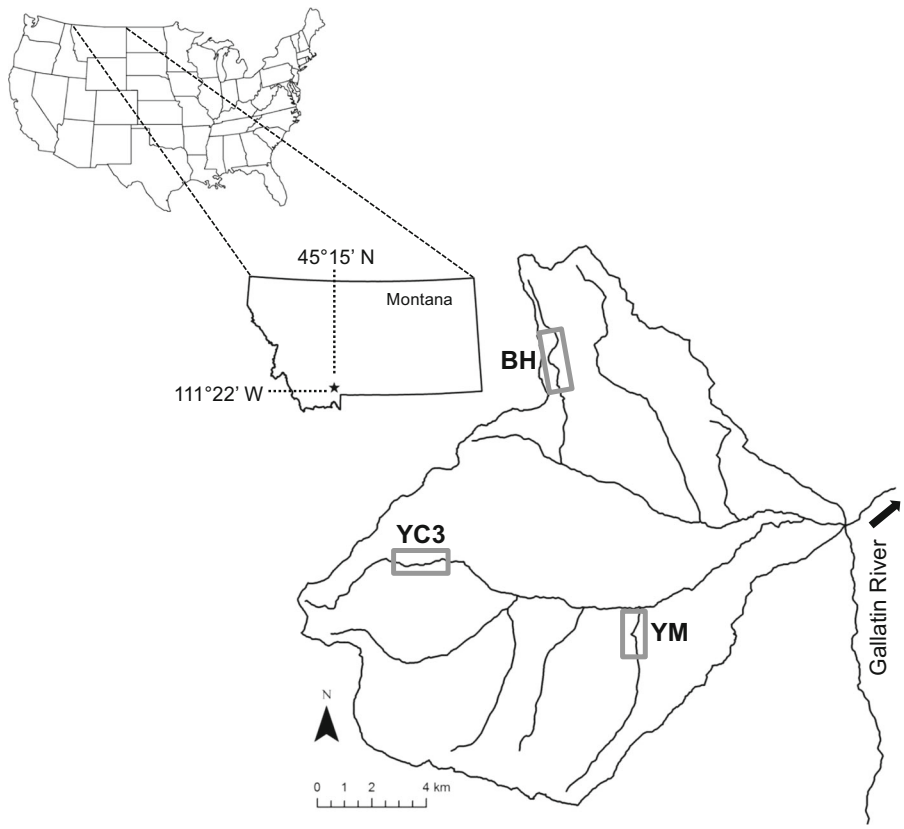

Fig. 1 Location of the West Fork of the Gallatin River watershed in southwestern Montana; and smaller scale map of the West Fork watershed showing the locations of the three study reaches: *BH* Beehive Creek, *YM* Yellow Mule Creek, *YC3* headwaters of the South Fork (reaches not to scale). USA map credit: worldatlas.com

Table 1 Physical and chemical characteristics of the three sites at which nutrient additions were performed

Site	Date	Drainage area (km^2)	Discharge ($L\ s^{-1}$)	Distance (m)	Temperature (°C)	Width (m)	Slope (%)	[NO_3-N] ($\mu g\ L^{-1}$)	[PO_4-P] ($\mu g\ L^{-1}$)	NO_3-N:PO_4-P (mass)	NO_3-N:PO_4-P (molar)
BH	11–12 Aug 2010	5.7	41–44	600	9.7 (1.4)	2.7	3.3	21 (12)	5.3 (4.0)	4.5 (1.3)	10 (2.9)
YM	17–18 Aug 2010	14	46–49	366	7.8 (1.7)	3.0	5.5	27 (2.1)	1.2 (0.52)	27 (12)	59 (26)
YC3	24 Aug 2010	9.6	37	450	8.2 (1.6)	3.2	5.8	15 (2.5)	0.39 (0.04)	37 (8.0)	82 (18)

Ambient dissolved nutrient concentrations and ratios on the days of the experiments are given as means with standard deviations in parentheses ($n = 4$ for dissolved nutrient samples; temperature standard deviations are based on 1-min interval logger samples during the experiment)

headwaters of the South Fork (YC3) is a first-order stream running through an undeveloped canyon draining a 9.6 km^2 watershed containing forest cover. Experimental stream reaches ranged from 366 m to 600 m in length, but were generally similar in average width, slope, water temperature, and discharge (Table 1). Benthic sediments in all streams consisted largely of cobble and gravel substrates, with small contributions of sand, silt, and clay. Benthic epilithic communities consisted of a relatively thin biofilm layer, largely composed of closely adhering diatoms (Piper, personal observation) Ambient nutrient concentrations were low at all three sites (Table 1), including very low concentrations of dissolved organic carbon (0.04–0.08 mg L^{-1}) and nitrogen (0.02–0.04 mg L^{-1}; McGlynn and Cross, unpublished data).

Experimental design

We examined coupled nitrate–nitrogen (NO_3-N) and phosphate phosphorus (PO_4-P) uptake patterns across a range of stoichiometric conditions. Our study streams were selected to encompass the range of ambient N:P ratios observed in headwater streams across the West Fork watershed (McGlynn and Cross, unpublished data), both within the dissolved nutrient pool (e.g., NO_3-N:PO_4-P; Table 1) and within benthic epilithic biomass (Table 2). An identical series of experiments was conducted at each of the three study reaches during summer baseflow conditions. There were no significant storms or high-flow events during our study.

Is it important to note that significant uptake, especially of phosphorus, can occur via sorption to fine sediments. Our methods described here are not able to separate abiotic removal vs. uptake by active biota. Thus, our conclusions about biotic uptake of phosphorus should be viewed with this limitation in mind.

Reach characterization

Prior to nutrient addition experiments, reaches were surveyed and stream width measured at 12 evenly spaced transects along each of the three experimental reaches. Water depth was measured at 10–20 points across the stream channel at each of the 12 transects. We collected streamwater grab samples at four locations along each reach—at the upstream end

Table 2 Characteristics of the bulk epilithic assemblage at each site

Site	AFDM (mg cm^{-2})	Chl *a* (μg cm^{-2})	% OM	% C (mass)	% N (mass)	% P (mass)	C:N (mass)	C:N (molar)	C:P (mass)	C:P (molar)	N:P (mass)	N:P (molar)
BH	0.40 (0.20)	0.46 (0.13)	61 (18)	16 (7.6)	1.7 (0.97)	0.22 (0.076)	9.9 (1.5)	12 (1.7)	71 (11)	180 (29)	7.3 (1.9)	16 (4.1)
YM	0.34 (0.05)	0.75 (0.16)	32 (9.8)	26 (3.3)	2.1 (0.42)	0.20 (0.058)	13 (1.2)	15 (1.4)	140 (56)	370 (140)	12 (5.3)	25 (12)
YC3	0.25 (0.05)	0.28 (0.02)	53 (9.6)	6.4 (0.054)	0.61 (0.16)	0.14 (0.019)	11 (3.4)	13 (3.9)	45 (6.1)	120 (16)	4.4 (1.2)	9.6 (2.7)

Values given are means, with standard deviations in parentheses ($n = 4$)

(head), at 25 and 50% of the experimental reach distance, and at the downstream end (base)—to characterize ambient concentrations of NO_3-N, PO_4-P, chloride (Cl), and bromide (Br). Ambient streamwater samples were stored on ice for transport to the laboratory, filtered within 24 h and frozen until analysis (see "Sample analysis" section).

We collected benthic epilithon samples at the same four locations in each reach. At each location, three rocks were selected haphazardly and scrubbed into a bucket of streamwater with a stiff plastic brush. The combined slurry from these rocks was collected in a sealed plastic bag and stored below 4 °C for transport to the laboratory. Rocks were photographed in the field using a metric ruler for scale, and rock surface areas were quantified via digital image analysis (ImageJ, National Institutes of Health, Bethesda, Maryland, USA) following procedures outlined by Steinman et al. (2006).

Stream discharge

Immediately prior to each experiment, we used dilution gauging to measure stream discharge at the downstream and upstream ends of each experimental reach. A solution of 500 g of sodium chloride (NaCl) dissolved in streamwater was added as an instantaneous injection (i.e., pulse) 40 m upstream of the measurement location to ensure complete mixing. Specific conductance (SC) was measured at 2-s intervals at each measurement location using Campbell Scientific CS547A temperature and conductivity probes logged to Campbell Scientific CR1000 data loggers (Logan, Utah, USA). The measured relationship between SC and NaCl concentration was used to estimate tracer dilution and to calculate discharge (Q) from the integrated NaCl breakthrough curve.

Experimental additions: single nutrient

At each reach, we conducted independent (separated in time) pulsed additions of NO_3-N and PO_4-P alongside additions of a conservative tracer (Cl) to estimate uptake rates of each nutrient relative to the conservative tracer following the methods described by Covino et al. (2010a). We first dissolved 1210 g Cl as NaCl and 41.6 g NO_3-N as potassium nitrate (KNO_3) in a bucket with stream water. We then poured the bucket contents carefully into the stream at the

head of the reach over the course of a few seconds. The mass of conservative tracer added was intended to cause a measurable increase in stream conductivity and quantification of the conservative Cl tracer across the breakthrough curve, while the mass of added nutrient was intended to raise in-stream nutrient concentrations to likely saturating levels for these oligotrophic headwater systems [>500 μg NO_3-N L^{-1} (Lohman et al. 1991; Covino et al. 2012); >100 μg PO_4-P L^{-1} (Bothwell 1989)]. Specific conductivity was measured at 2-s intervals for the duration of the experiment. We collected grab samples at the downstream end of each reach over the entire breakthrough curve, with sampling frequency ranging from 30 s to 10 min depending on the rate at which SC (and therefore tracer concentration) was changing, resulting in 22–26 samples per experimental addition. Experiments typically lasted 1–3 h. Samples were stored on ice for transport to the laboratory, filtered within 24 h and frozen until analysis as described previously.

Once the NO_3-N pulse had fully cleared the reach (i.e., after a return to background conductivity), we conducted a similar addition of PO_4-P, using 1210 g Cl as NaCl and 13.7 g PO_4-P as potassium phosphate (KH_2PO_4) dissolved in stream water. Samples were collected and analyzed as described above for NO_3-N tracer additions in each reach. While we cannot be certain that our P addition was not influenced by the prior N addition, the time between additions (at least 1 h) was likely sufficient to remove most of the nitrogen from the dominant flow paths.

Calculating uptake rates: single nutrient

Data from single nutrient additions were analyzed using the TASCC method (Covino et al. 2010a), which allows estimation of uptake rates across a wide range of nutrient concentrations during a single stream tracer experiment. This method has produced comparable results to classical steady-state approaches (Powers et al. 2009, Covino et al. 2010a, 2012) but allows for full kinetic curve estimation (i.e., nutrient uptake as a function of concentration) from one experiment rather than uptake in response to a single concentration (also see Trentman et al. 2015). The TASCC method compares the ratio of added nutrient (i.e., NO_3-N or PO_4-P, represented by X) to added conservative tracer (e.g., Cl) in each grab sample to the injectate ratio. The slope of the natural logarithms of these ratios plotted against stream distance yields an estimate of added nutrient longitudinal uptake rate ($k_{w\text{-}add\text{-}X}$) for each sample on the downstream breakthrough curve. The negative inverse of $k_{w\text{-}add\text{-}X}$ is the added nutrient uptake length ($S_{w\text{-}add\text{-}X}$) for each sample. $S_{w\text{-}add\text{-}X}$ is used to calculate the added nutrient areal uptake rate ($U_{add\text{-}X}$) for each sample collected as:

$$U_{add-X} = \frac{Q \times [X_{add}]}{w \times S_{w-add-X}}, \quad (1)$$

where Q is stream discharge, $[X_{add}]$ is the geometric mean of observed (background corrected) and 'conservative' concentrations of nutrient X in a grab sample, w is average wetted stream width for the experimental reach, and $S_{w\text{-}add\text{-}X}$ is the uptake length of added nutrient X for a given grab sample. The 'conservative' concentration represents the amount of nutrient X that would have been present in a breakthrough curve sample if no uptake had occurred along the reach, and is calculated as the product of observed Cl concentrations (background corrected) and the X:Cl ratio in the injectate.

We calculated ambient uptake length ($S_{w\text{-}amb\text{-}X}$) for each experiment by regressing the $S_{w\text{-}add\text{-}X}$ values against total nutrient concentration (X_{tot}) and back-extrapolating to ambient concentration (Payn et al. 2005; Covino et al. 2010a). Ambient areal uptake rate ($U_{amb\text{-}X}$) is then calculated from $S_{w\text{-}amb\text{-}X}$:

$$U_{amb-X} = \frac{Q \times [X_{amb}]}{w \times S_{w-amb-X}}, \quad (2)$$

where Q is stream discharge, X_{amb} is the ambient X concentration, w is average wetted stream width for the experimental reach, and $S_{w\text{-}amb\text{-}X}$ is the ambient uptake length for nutrient X.

Total nutrient uptake for each grab sample during an experiment is equal to the sum of ambient and added nutrient uptake:

$$U_{tot-X} = U_{amb-X} + U_{add-X}, \quad (3)$$

where $U_{tot\text{-}X}$ is the total uptake rate of nutrient X for each grab sample, $U_{amb\text{-}X}$ is the ambient uptake rate of nutrient X, and $U_{add\text{-}X}$ is the uptake rate of added nutrient X for that sample. It is important to note that $U_{add\text{-}X}$ only represents the uptake of added nutrient, that $U_{amb\text{-}X}$ is the calculated uptake occurring in the absence of added nutrient, and that $U_{tot\text{-}X}$ is the total of added and ambient reach uptake.

Models of nutrient uptake kinetics: single-nutrient

Dugdale (1967) applied the Michaelis–Menten (M–M) model of enzyme kinetics to describe nutrient uptake kinetics of marine algae in laboratory experiments:

$$U_{tot-X} = \frac{U_{max-X} \times C}{K_{m-X} + C}, \quad (4)$$

where $U_{tot\text{-}X}$ is the areal uptake rate of nutrient X at concentration C, $U_{max\text{-}X}$ is the maximum uptake rate of nutrient X, and $K_{m\text{-}X}$ is the half-saturation constant, or the concentration of X at which $U_{tot\text{-}X}$ is equal to $\frac{1}{2}U_{max\text{-}X}$. This model has since been extended to examine ecosystem-level nutrient uptake in freshwater systems, including streams and rivers (e.g., Earl et al. 2006; Demars 2008; O'Brien and Dodds 2010; Covino et al. 2010a, b, 2012). We fit the M–M model to our uptake-concentration data to estimate $U_{max\text{-}X}$ and $K_{m\text{-}X}$ for each nutrient experiment. The M–M kinetic model also allowed for estimation of uptake rates at a series of benchmark concentrations for inter-site comparison of uptake rates at comparable [X]. When the M–M model did not fit the data (e.g., linear response in the P-only addition at YM), we parameterized an efficiency-loss model (O'Brien et al. 2007):

$$U_{tot-X} = a \times C_X^b, \quad (5)$$

where $U_{tot\text{-}X}$ is the areal uptake rate at nutrient concentration C_X, and a and b are constants ($b < 1$). While this model does not allow estimation of $U_{max\text{-}X}$ or $K_{m\text{-}X}$, it does allow estimation of uptake rates at benchmark concentrations to facilitate comparison among sites.

Experimental additions: dual-nutrient

We also conducted time-lagged additions of both NO_3-N and PO_4-P with associated conservative tracers (Cl and Br) at each study reach within 24 h of the individual nutrient experiments described above to quantify interactions and synergies between the availability and uptake of these two nutrients across a ranges of concentration and stoichiometry. We released a solution of 1210 g Cl as NaCl and 41.6 g NO_3-N as KNO_3 in stream water as an instantaneous pulse at the head of the reach. Five to six minutes later, depending on travel time in the experimental reach, we released a second instantaneous pulse containing 134 g Br as potassium bromide (KBr) and 13.7 g PO_4-P as KH_2PO_4 at the head of the reach. At each experimental stream reach, the time lag between the two pulse additions was set to approximately half of the time to peak concentration at the downstream end of the reach as observed in a previous tracer addition (6 min at BH and YC3; 5 min at YM), in order to maximize variability in dissolved NO_3-N:PO_4-P concentrations and ratios experienced by the stream during the experiment. Samples were collected and analyzed in the same fashion as described previously for the single-nutrient additions (see "Appendix").

Based on observed Cl concentrations and the total masses of Br added as KBr in the dual-nutrient experiments, the measured Br concentrations in the grab samples were consistently lower than expected, suggesting malfunction during the analytical procedure. To enable subsequent analyses, we estimated Br concentrations from the Cl concentrations measured during the same dual experiment. To do this, we shifted the Cl breakthrough curve forward by the length of time between the two solute additions for each dual experiment (6 min at BH and YC3; 5 min at YM). We then used the ratio of the total mass of Br added to the total mass of Cl added in that experiment to estimate corresponding Br concentrations over time. This substitution did not adversely affect the resulting calculations as both Cl and Br behave conservatively in low background stream systems. Furthermore, due to the short duration of these experiments during baseflow, it is highly unlikely that flowpaths and rates changed significantly over the five-to-six minute time-lag, making this an effective method for estimating the Br concentrations needed to calculate P uptake in this experiment.

Calculating uptake rates: dual-nutrient

Uptake rates for each nutrient during the dual additions were also calculated according to the TASCC method (Covino et al. 2010a; Eqs. 1–3). Calculations for each nutrient were based only on the concentrations of that same nutrient (e.g., estimates of $U_{tot\text{-}N}$ did not include PO_4-P concentrations). Because concentrations of both nutrients were changing during each dual-nutrient addition, back-extrapolating to the ambient streamwater concentration of one nutrient did not

yield a true value of U_{amb}. However, we still chose to include this calculation for our dual-nutrient additions.

Models of nutrient uptake kinetics: dual nutrient

To capture the influence of the concentration of a second nutrient on uptake rates of the first, we considered the experimental data in three dimensions. We adapted Megee et al.'s (1972) model describing microbial growth as a function of two limiting nutrients. Our model allowed us to calculate 'stoichiometric uptake surfaces' that may be used to predict uptake of N or P across a range of nutrient concentrations and N:P ratios. This model incorporated the measured concentrations and calculated dynamic uptake rates of NO_3-N and PO_4-P from both the single-and dual-nutrient additions (see Fig. 2 for a conceptual explanation). To our knowledge, this effort represents the first application of this approach at the ecosystem-level. The model is essentially an extension of the Monod equation (Monod 1950) that includes another term to incorporate a second nutrient:

$$U_{tot-X} = U_{max-X} \times \frac{C_N}{K_{m-N} + C_N} \times \frac{C_P}{K_{m-P} + C_P}, \quad (6)$$

where $U_{tot\text{-}X}$ is the total areal uptake rate of nutrient X (i.e., NO_3-N or PO_4-P), $U_{max\text{-}X}$ is the maximum areal uptake rate of that same nutrient X, C_N and C_P are the concentrations of NO_3-N and PO_4-P, respectively, and $K_{m\text{-}N}$ and $K_{m\text{-}P}$ are the half-saturation constants for NO_3-N and PO_4-P, respectively.

Where this model did not fit the data (i.e., for P uptake at YM), we instead applied a dual-substrate efficiency-loss model, that we developed by extending the power law form to include a second term:

$$U_{tot-X} = a \times C_N^b \times C_P^c, \quad (7)$$

where $U_{tot\text{-}X}$ is the total areal uptake rate of nutrient X, C_N and C_P are the concentrations of NO_3-N and PO_4-P, respectively, and a, b, and c are constants ($b < 1$ and $c < 1$).

Sample analysis

Background streamwater and stream tracer addition breakthrough curve samples were placed on ice, filtered with 0.45 µm polyethersulfone syringe filters (Environmental Express, Charleston, South Carolina, USA) within 2–6 h of field collection, and stored at −20 °C until analysis. Samples were analyzed for NO_3-N, PO_4-P, Cl, and Br on a Metrohm Peak model 820 ion chromatograph (IC) equipped with a 4 mm × 250 mm A-supp anion exchange column (Metrohm, Herisau, Switzerland). IC detection limits were 0.01 mg NO_3-N L^{-1}, 0.01 mg PO_4-P L^{-1}, 0.01 mg Cl L^{-1}, and 0.01 mg Br L^{-1}. Samples collected near the tails of the breakthrough curves were often below the IC detection limits for NO_3-N and PO_4-P. Replicate samples at these tails were analyzed via colorimetry (ascorbic acid method) using a SEAL QuAAtro segmented flow analyzer (SEAL Analytical, Mequon, Wisconsin, USA; 10 mm path length), which had detection limits of ~0.3–0.4 µg L^{-1} NO_3-N and PO_4-P.

Two subsamples from each epilithic slurry were filtered onto pre-ashed GF/F glass microfiber filters (0.7 µm pore size; Whatman, Kent, UK). One of these

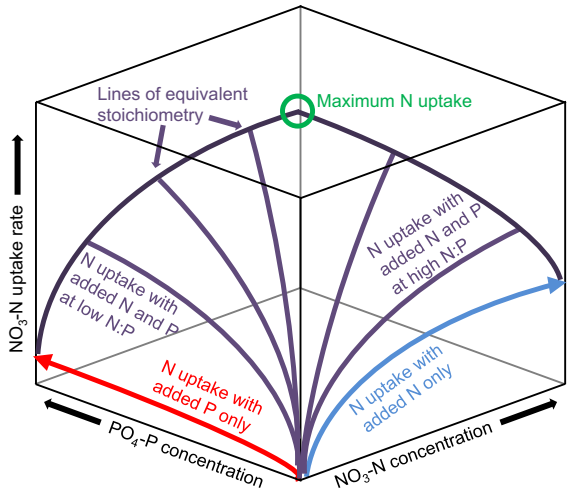

Fig. 2 Conceptual diagram outlining the construction of a three-dimensional plot of dual-nutrient uptake kinetics. The *light blue line* represents NO_3-N uptake with the addition of NO_3-N alone. This relationship is the same as that developed during a single nutrient addition. The *red line* represents NO_3-N uptake with the addition of PO_4-P alone. This relationship is purely theoretical, but we might expect NO_3-N uptake rates to increase slightly with increased PO_4-P availability, as this addition would relieve P limitation and allow more N to be utilized. The *light purple lines* represent NO_3-N uptake with the addition of both NO_3-N and PO_4-P at constant ratios. Adding both nutrients together results in increased NO_3-N uptake, regardless of the ratio. The *green circle* shows that maximum NO_3-N uptake occurs when large amounts of both NO_3-N and PO_4-P are added at a moderate ratio, which would relieve any potential limitation by these two nutrients

filters was oven-dried at 60 °C to a constant mass, weighed, combusted in a muffle furnace at 500 °C for 2.5 h, and reweighed to quantify ash-free dry mass (AFDM). The other filter was stored at −20 °C until analysis of chlorophyll *a*, at which time chlorophyll was extracted from the filters with acetone and quantified using the fluorometric acidification method (Steinman et al. 2006). The remaining slurry was centrifuged, decanted, frozen, freeze-dried, and subsampled for analysis of carbon (C), nitrogen (N), and phosphorus (P) content. Percent C and N were analyzed using a PDZ Europe ANCA-GSL elemental analyzer (Sercon Ltd., Cheshire, UK) at the University of California-Davis Stable Isotope Facility. Peach leaves and glutamic acid were used as external standards for C and N analyses, respectively (99% recovery for C, 101% recovery for N). Percent P was analyzed by acid persulfate digestion (APHA 1998). Wheat was used as an external standard for P analysis (mean recovery 89%). Stoichiometric data are presented as mass ratios to facilitate direct comparisons with uptake rates; however, molar ratios are shown in Table 1 for comparison.

Statistical analyses

All background data (e.g., dissolved nutrients, AFDM) are presented as means and standard deviations of the samples collected at each experimental reach. Two-dimensional model fits (M–M and efficiency-loss) were conducted in SigmaPlot 10.0 (Systat Software, Inc., San Jose, CA, USA) and include 95% confidence intervals. Three-dimensional model fits (adapted Megee and efficiency-loss models) were conducted in MatLab R2010b (MathWorks, Natick, MA, USA). All model fits were constructed by interactively solving the appropriate equation for parameter values that minimized the sum of the squared differences between observed and predicted values.

Results

Physical, chemical, and biological characteristics of the experimental streams

Environmental conditions, including stream discharge, were similar across experimental tracer additions and reaches (Table 1). Ambient nutrient concentrations were low, but somewhat variable across sites (Table 1). Dissolved nutrient ratios (i.e., NO_3:PO_4) ranged from 4.5:1 (mass ratio) at BH to 37:1 at YC3 (see Table 1 for molar ratios).

Standing stocks of epilithic biomass were relatively low at all sites. Epilithic organic matter ranged from 0.25–0.40 mg AFDM cm^{-2}, while epilithic chlorophyll *a* ranged from 0.28–0.75 μg cm^{-2} (Table 2). Both epilithic organic matter and chlorophyll *a* were lowest at YC3 (Table 2). The autotrophic index (i.e., AFDM:Chlorophyll *a*; an index of relative autotrophy within biofilms) in YM was nearly half that of BH and YC3 (mean: YM = 0.45; BH = 0.87; YC3 = 0.89).

Epilithic nutrient contents and stoichiometry varied considerably among the study sites (Table 2). Epilithic carbon content showed the highest variation among reaches, followed by nitrogen and phosphorus content (Table 2). Relatively high nutrient contents resulted in low epilithic C:N and C:P (Table 2). Epilithic C:P varied widely across the three sites, driven primarily by variation in %C (Table 2), whereas C:N was relatively similar among sites. Inter-site differences in epilithic %N and %P led to variable N:P, ranging from 4.4:1 (mass) at YC3 to 12:1 at YM (Table 2).

Patterns of nutrient uptake kinetics

Single-nutrient additions

Ambient nutrient uptake rates ($U_{amb\text{-}N}$ and $U_{amb\text{-}P}$) during single-nutrient pulses varied among sites and were consistently higher for N than P (Table 3). Ambient NO_3-N uptake rates were highest at YM and lowest at YC3, and inter-site differences in uptake paralleled differences in NO_3-N concentrations and %N of epilithon (Tables 1, 2, 3). Ambient PO_4-P uptake rates were ~2- to 10-fold lower than NO_3-N, and inter-site differences in these rates were also consistent with differences in PO_4-P concentrations and %P of epilithon (Tables 2, 3). Ambient NO_3-N and PO_4-P uptake rates were strongly and positively correlated ($r = 0.98$, $p < 0.001$) across sites and dates. Uptake N:P stoichiometry at ambient concentrations ($U_{amb\text{-}N}$:$U_{amb\text{-}P}$) varied between 2.3:1 to 11:1, and there was no apparent relationship between uptake N:P stoichiometry and N:P ratios of either epilithic biomass or streamwater (Tables 2, 3).

Table 3 Back-extrapolated ambient uptake rates and M–M model parameters for individual and dual slugs of NO_3-N and PO_4-P at BH, YM, and YC3

Site	Date	Slug	NO_3			PO_4			$U_{amb\text{-}N}$:$U_{amb\text{-}P}$ (by mass)
			$U_{amb\text{-}N}$ (μg N m^{-2} min^{-1})	$U_{max\text{-}N}$ (μg N m^{-2} min^{-1})	$K_{m\text{-}N}$ (μg N L^{-1})	$U_{amb\text{-}P}$ (μg P m^{-2} min^{-1})	$U_{max\text{-}P}$ (μg P m^{-2} min^{-1})	$K_{m\text{-}P}$ (μg P L^{-1})	
BH	11 Aug 2010	Individual	10	410	390	4.3	1700	870	2.3
BH	12 Aug 2010	Dual	170	570	96	35	580	130	4.9
YM	17 Aug 2010	Individual	37	770	560	3.4	[a]	[a]	11.1
YM	18 Aug 2010	Dual	54	860	380	7.1	1400	180	7.6
YC3	24 Aug 2010	Individual	4.0	500	1300	0.97	780	320	4.1
YC3	24 Aug 2010	Dual	6.7	640	940	2.5	640	150	2.7

The mass ratios of ambient uptake rates are also given

[a] The individual PO_4 slug at YM did not follow Michaelis–Menten kinetics. An efficiency-loss model was applied instead to generate estimates of uptake rate at ambient and additional benchmark concentrations. For YM PO_4, $U = 4.7 \times [PO_4\text{-}P]^{0.99}$

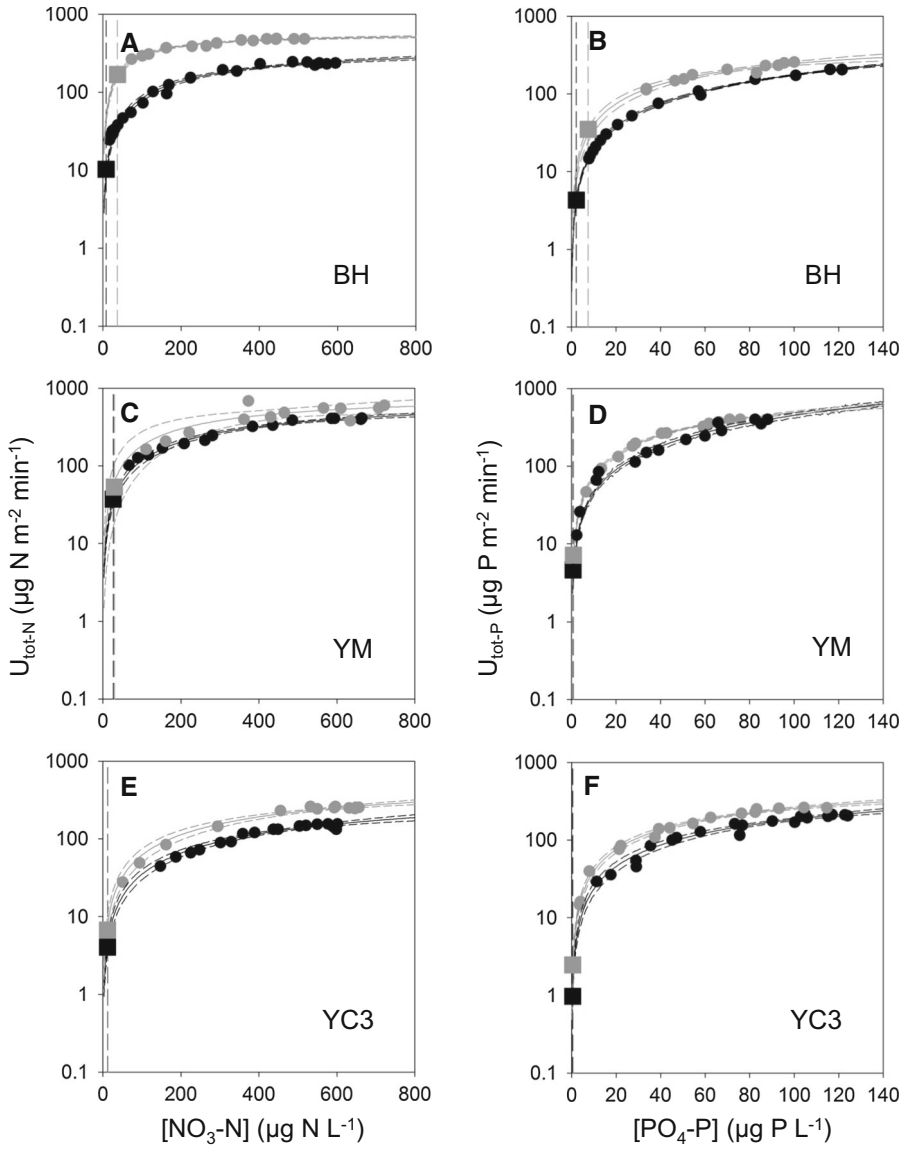

Fig. 3 Uptake kinetic curves during the nutrient addition experiments conducted at each site. Single nutrient additions (i.e., N or P alone) are shown in *black*, and dual-nutrient additions (i.e., N and P together) are shown in *gray*. *Points* represent grab samples collected during the breakthrough curve. *Solid lines* represent the Michaelis–Menten (M–M) model fit, with 95% confidence intervals shown as *dashed lines* around those fits. The back-extrapolated uptake rate at ambient nutrient concentrations is indicated by the *square*, and the *vertical dashed lines* correspond to ambient nutrient concentrations. Note that ambient concentrations of dissolved NO_3-N and PO_4-P were slightly higher during the dual slug

Relationships between nutrient concentrations and uptake rates during experimental additions generally followed M–M kinetics, however differences in ecosystem-level responses to added nutrients were apparent among sites (Fig. 3: black circles, Table 3). With respect to N uptake, BH exhibited the most dramatic initial response to the pulsed addition of N (steepest initial slope and lowest $K_{m\text{-}N}$; Table 3, Fig. 3) but saturated at maximum uptake values that were lower than YM or YC3 ($U_{max\text{-}N}$; Fig. 3, Table 3). In contrast, YM and YC3 were less responsive to added N (gentler initial slope and higher $K_{m\text{-}N}$ values; Fig. 3, Table 3), but maximum uptake rates were ~25–90% higher than in BH. Phosphorus uptake rates also varied strongly with concentration and showed differences in response to, and capacity for (i.e., maximum uptake) added P (Table 3; Fig. 3). YM had the highest maximum P uptake values, but data at this site did not follow M–M kinetics (i.e., no $U_{max\text{-}P}$ value; Fig. 3: black circles, Table 3). P uptake kinetics at BH and YC3 differed in that BH was less responsive to added P, but had a higher maximum uptake rate. In general, streams with high responsiveness to N (low $K_{m\text{-}N}$; e.g., BH) showed low responsiveness to P (high $K_{m\text{-}P}$). Maximum rates of uptake ($U_{max\text{-}P}$ and $U_{max\text{-}N}$) were not correlated.

Dual-nutrient additions

Addition of a second nutrient consistently led to elevated uptake of either NO_3-N or PO_4-P across all measured nutrient concentrations at all sites (Fig. 3: grey circles). Both ambient and maximum uptake of N were higher when P was added, while $K_{m\text{-}N}$ values were lower, indicating steeper kinetic curves that saturated at higher N uptake rates during the dual-nutrient additions at all sites (Fig. 3; Table 3). Addition of N similarly resulted in higher $U_{amb\text{-}P}$ and lower $K_{m\text{-}P}$ for PO_4-P at all sites (Table 3). In contrast, maximum P uptake rates were higher during the single additions at BH and YC3, but this was likely due to model extrapolation beyond the measured range of nutrient concentrations.

We used the fitted, single element models from each experiment to compare single nutrient uptake when it was added alone to uptake of the same nutrient in the presence of the other nutrient (during dual additions) across a series of benchmark concentrations within our measured uptake data range (i.e. not model-extrapolated; Fig. 4). Uptake rates were consistently higher during the dual additions, but the magnitude of increase varied between nutrients and among sites. At nutrient concentrations that represent average ambient concentrations across the three sites (20 μg NO_3-N L^{-1} and 2.0 μg PO_4-P L^{-1}), BH showed a 500% increase in $U_{tot\text{-}N}$ with added P, but only a 230% increase in $U_{tot\text{-}P}$ with added N. At the other two sites, uptake of N and P were similarly stimulated ($\sim$160–180%) with the addition of the second nutrient at these average ambient concentrations (Fig. 4). The proportional increases in uptake declined at higher concentrations at BH and YM, but showed no change at higher concentrations at YC3 (Fig. 4). Uncertainty in all benchmark uptake estimates was relatively low (i.e., small 95% confidence intervals; Fig. 3).

Inferences from two-dimensional uptake plots are limited because they do not show how variability in nutrient concentrations *and* ratios affect uptake dynamics (Figs. 3, 4). In contrast, our dual-nutrient kinetic models, and the resulting stoichiometric response surfaces (Fig. 5; Table 4), characterize how interactions between NO_3-N and PO_4-P availability influence uptake dynamics simultaneously. Stoichiometric surfaces show that sites differed in their responses to added N or P, and that the dependence of nutrient uptake on the supply of the additional nutrient varied across sites, concentrations, and ratios (Fig. 5). Nitrogen uptake rates were clearly most responsive to added P at BH, and the model surface at this site was more symmetrical than surfaces derived for the other sites (Fig. 5c, e). Nitrogen surfaces at YM and YC3 showed that N uptake rates were much less responsive to added P, regardless of N concentration (Fig. 5c, e). Phosphorus uptake rates were also positively influenced by N addition, but this response was only obvious in YM when P concentrations were elevated (Fig. 5d). In general, the influence of P concentration on N uptake was much stronger than the influence of N concentration on P uptake (Fig. 5b, d, f).

Response surfaces demonstrated that uptake of either nutrient was more strongly influenced by the other at relatively low nutrient concentrations. For instance, the effect of additional P on $U_{tot\text{-}N}$ was most evident at low P concentrations (i.e., $\sim$10–30 μg L^{-1} PO_4-P; Fig. 5a, c, e). Generally lower values of $K_{m\text{-}P}$ than $K_{m\text{-}N}$ in surface models of $U_{tot\text{-}N}$ at all three reaches further support this rapid response of $U_{tot\text{-}N}$ to even slight increases in P availability (Table 4). Similar patterns were seen for $U_{tot\text{-}P}$ relative to changes in N concentrations at all three reaches (Fig. 5; Table 4). For all three reaches, the greatest uptake of both N and P occurred when both nutrients were at maximum concentration (Fig. 5).

Discussion

Nutrient uptake and colimitation at the ecosystem level

Nutrient limitation of ecosystems has been assessed using a wide variety of techniques and perspectives (e.g., Chapin et al. 1986; Howarth 1988; Sterner and Hessen 1994). In streams and lakes, short-term bioassays have been used extensively, in which biomass growth of the microbial community is quantified in response to elevated nutrient concentrations, either through spiked additions of dissolved nutrients or benthic nutrient-diffusing substrata (Francoeur 2001; Elser et al. 2007). In streams, the development of whole-system nutrient spiraling methods (Mulholland and Webster 2010) has enabled a suite of integrated metrics of system-level nutrient uptake and demand (Webster and Valett 2007).

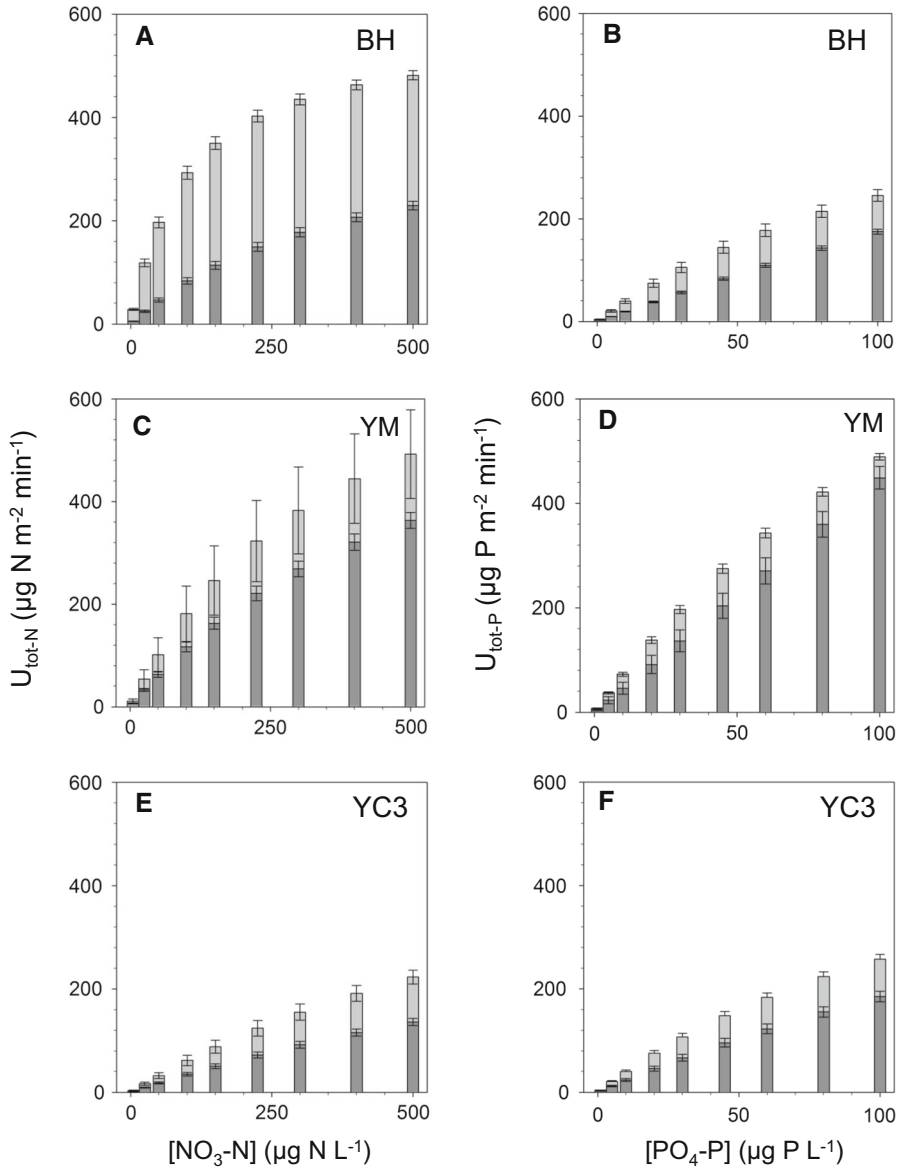

Fig. 4 Uptake rates at benchmark concentrations calculated from the kinetic model for each slug addition at each site. Uptake during single slugs are shown in *dark gray*, with increases in uptake during dual slugs shown in *light gray*. *Error bars* represent the 95% confidence interval for each estimate

Although uptake of nutrients from the water column is a distinctly different process than biomass growth, it is typically assumed that immediate uptake of nutrients during short-term experiments (i.e., minutes to hours) is strongly correlated with future biomass growth. In this context, we can view our short-term experiments as a proxy for how nutrient availability may influence benthic stream productivity. Our results thus suggest that (a) productivity of our study streams is both limited individually by NO_3-N and PO_4-P and colimited by both of these nutrients, and (b) uptake of either nutrient (i.e., N or P) is strongly coupled to the availability of the other. However, because nutrient uptake was our measured response variable—versus

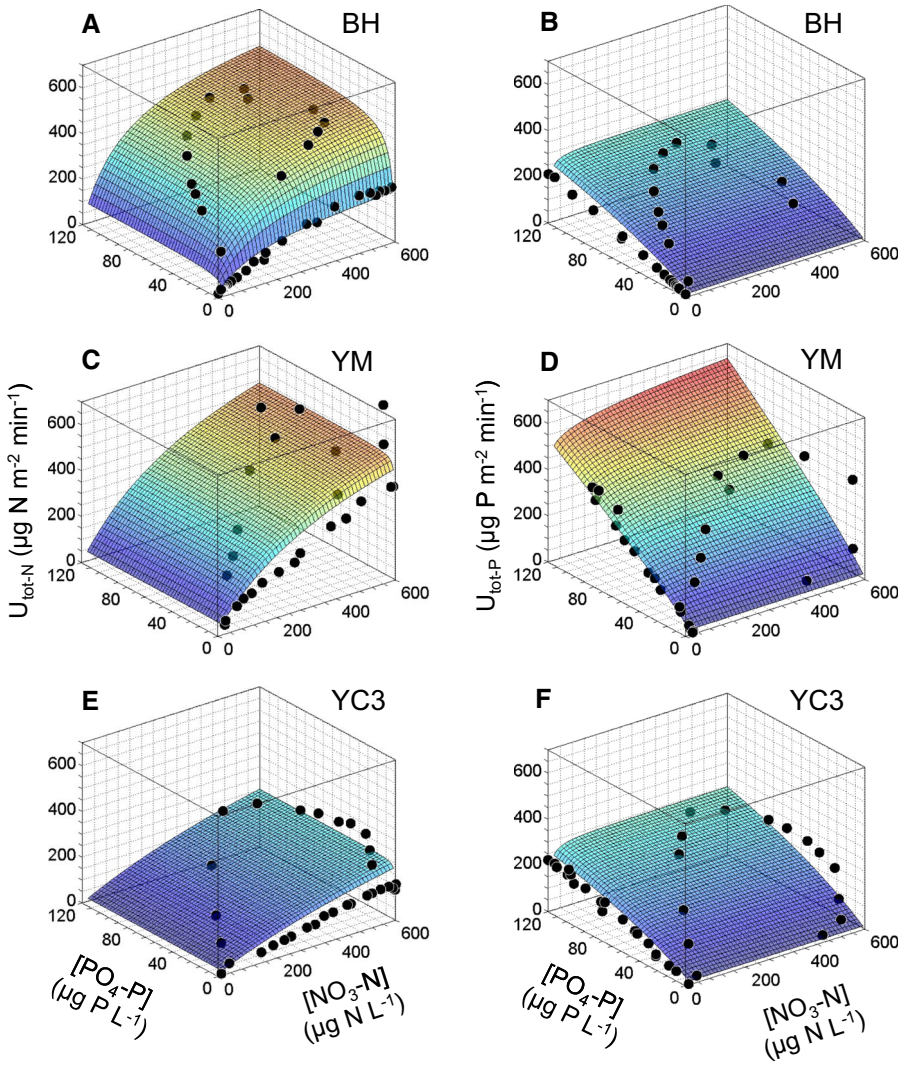

Fig. 5 The stoichiometry of uptake for NO_3-N and PO_4-P at each site. *Points* represent grab samples from both individual and dual slugs

biomass growth—our results cannot be directly assessed in the context of nutrient limitation metrics developed from classical bioassay approaches (e.g., synergistic limitation vs. sequential limitation; Elser et al. 2009; simultaneous colimitation vs. independent colimitation; Harpole et al. 2011). Future research should aim to better align various long-term and short-term methods for quantifying nutrient limitation (see King et al. 2014).

At all three of our sites we observed elevated uptake rates with increasing concentrations of both N and P (Figs. 3, 4). In general, $U_{tot\text{-}N}$ and $U_{tot\text{-}P}$ increased rapidly with concentration, but tended to level off at the highest concentrations (i.e., following M–M dynamics). These patterns suggest that our study streams are not saturated with respect to either N and P loading (Bernot and Dodds 2005), and that the existing biotic community maintains the capacity to temporarily remove or dampen nutrient pulses from the landscape (e.g., Rier et al. 2016). Other research in this same watershed (Covino et al. 2012) has shown that streams draining watersheds with more suburban development tend to support higher epilithic biomass and consequently higher uptake capacities, or U_{max} values. Thus, as streams become more nutrient-rich, the development of active microbial biomass could

Table 4 Two-substrate M–M parameters for the stoichiometry of uptake at each site

Site	Nutrient	$U_{max\text{-}X}$ (μg N or P m^{-2} min^{-1})	$K_{m\text{-}N}$ (μg N L^{-1})	$K_{m\text{-}P}$ (μg P L^{-1})
BH	NO_3	670	140	3.2
BH	PO_4	850	4.1	230
YM	NO_3	920	420	0.27
YM	PO_4	[a]	[a]	[a]
YC3	NO_3	690	1000	0.28
YC3	PO_4	770	5.1	190

[a] Since the individual PO_4 slug at YM did not follow Michaelis–Menten kinetics, a two-substrate efficiency-loss model was applied to generate a stoichiometric surface. For YM PO_4, $U = 6.2 \times [NO_3\text{-}N]^{0.07} \times [PO_4\text{-}P]^{0.87}$

help to postpone potential downstream fluxes of elevated nutrients, alter the chemical form of nutrient flux (e.g., inorganic to organic), or permanently remove nutrients via processes such as denitrification. Indeed, NO_3-N concentrations across the West Fork of the Gallatin watershed are relatively low and uniform during the high biological activity summer months, despite the large spatial variability in land use and N loading (Gardner and McGlynn 2009; Gardner et al. 2011). During the low productivity winter months, nutrient concentrations are elevated and exhibit greater spatial variability (Gardner and McGlynn 2009). Such patterns suggest an important role for in-stream processes in removing or dampening N inputs delivered from the landscape (e.g., Bernhardt et al. 2003; Gardner et al. 2011). However, elevated non-point sources of nitrogen during the winter may also help explain elevated N concentrations during the winter. Regardless, streams in the West Fork watershed are still at risk of exceeding nutrient thresholds and saturating (sensu Aber et al. 1989) as development and land use change continues to grow in this mountain region (Hansen et al. 2002).

The shapes of uptake-concentration curves can provide information about how streams differ in their response to elevated nutrient concentrations (Covino et al. 2012). Relatively low $K_{m\text{-}X}$ values are consistent with a high affinity for nutrient X at the ecosystem-level (steeper kinetic curve), and these values may provide inference about spatial or temporal variability in nutrient limitation. As well, values of $U_{max\text{-}X}$ relate to the total capacity of the ecosystem to remove nutrients, and these values are expected to vary positively with whole-ecosystem metabolism. In our single-nutrient additions, $K_{m\text{-}N}$ values were lower in BH than YM or YC3, suggesting stronger N limitation and greater responsiveness to N availability in BH than the other two streams (Table 3). In contrast, $K_{m\text{-}P}$ was highest in BH, reflecting lower demand for P in BH under ambient N supply (Table 3). More relevant for our work, however, is the *change* in $K_{m\text{-}X}$ or U in response to the addition of a colimiting nutrient. In all cases, $K_{m\text{-}X}$ was reduced—sometimes drastically—by addition of the other nutrient (Table 3). In addition, most measurements of U ($U_{tot\text{-}N}$, $U_{tot\text{-}P}$, and $U_{max\text{-}N}$) were higher in the presence of the other nutrient. Thus, both the affinity and capacity for N and P uptake were enhanced by elevated concentrations of a colimiting nutrient. Only a few other studies have shown such strong coupling between N and P uptake at the ecosystem level (e.g., Schade et al. 2011; Gibson et al. 2015); yet, this result is likely to be general for streams that are far below nutrient saturation.

Although our dual-nutrient experiments revealed reciprocal influences between N and P availability and uptake, responses to experimental pulses were not always symmetrical. Ambient uptake ratios (Tables 2, 3) and relative increases in uptake during the dual nutrient additions (Fig. 4) both suggested that NO_3-N uptake in BH was more strongly limited by additions of PO_4-P than in the other two streams. Stoichiometric surfaces of dual-nutrient uptake allow further visualization of these varying, nonlinear limitation dynamics (Fig. 5). $U_{tot\text{-}N}$ at BH (Fig. 5a) showed the strongest response to altered availability of the second nutrient. In particular, when NO_3-N was readily available (>400 μg N L^{-1}) and PO_4-P was scarce (<10 μg P L^{-1}), even a small increase in PO_4-P concentration resulted in a dramatic increase in $U_{tot\text{-}N}$. Thus, any increase in availability of PO_4-P appeared to allow further utilization of readily available NO_3-N. The relative flatness of the BH $U_{tot\text{-}P}$ surface along the

NO_3-N axis lends further support to the PO_4-P limitation of this reach, as increased NO_3-N availability did little to stimulate $U_{tot\text{-}P}$ (Fig. 5b). In the other two streams, responses of N to P and P to N were generally more symmetrical, suggesting that these streams are more balanced with respect to colimitation by N and P. Future application of this approach should consider whether reversing the order of nutrient pulses (i.e., P before N vs. N before P) could influence the results and interpretation. For instance, demand for one nutrient could be more influenced by prior exposure to the other nutrient than by instantaneous concentrations, per se.

Although our interpretations have been based primarily on measured uptake kinetics, it is important to note that the uptake rates calculated from these experiments were in fact bulk removal rates, which can include nutrient removal by a number of pathways other than assimilatory uptake into biomass. For NO_3-N, one such pathway is denitrification, by which NO_3-N is converted to N_2 and lost from the system. While this process can be important in small headwater streams (Bernot and Dodds 2005), previous research in other relatively pristine systems in the mountain west found that denitrification accounted for less than 10% of total NO_3-N uptake (Mulholland et al. 2008); thus our NO_3-N uptake measurements likely reflect assimilatory uptake. For PO_4-P, the most important alternative removal pathway is abiotic sorption onto stream sediments (Reddy et al. 1999). Because it is technically difficult to separate removal by sorption from biological uptake (Powers et al. 2009), our absolute estimates of PO_4-P uptake rates should be viewed with some caution. Nonetheless, P sorption is expected to be relatively low at our study sites because of limited amounts of silt and clay. In addition, if we limit our inference to changes in $U_{tot\text{-}P}$ during the dual nutrient addition, we can assume that these increases were entirely due to higher biological demand for PO_4-P as a result of elevated NO_3-N availability. Indeed, there is no known mechanism by which elevated NO_3-N concentration would lead to increased PO_4-P sorption (Schade et al. 2011).

Relationships between biomass stoichiometry and nutrient uptake stoichiometry

If biotic demand is the primary driver of uptake dynamics, and nutrients are largely supplied from the water column (vs. alternative sources such as local mineralization), knowledge of assimilatory demand across microbial taxa and habitats should enable predictions about uptake patterns and stoichiometry (Cross et al. 2005). If we assume that the nutrient content of epilithon serves as a proxy for demand by the dominant assimilators, then epilithic stoichiometry should correlate with patterns of nutrient uptake. In our limited number of streams, there was no clear relationship between uptake N:P and epilithic N:P; however, we did find that YM had the highest values of both epilithic N:P *and* ambient uptake N:P (Tables 2, 3). In addition, inter-site differences in ambient uptake of NO_3-N and PO_4-P consistently mirrored the differences in %N and %P of epilithon. Interestingly, Gibson and O'Reilly (2012) similarly found that the N:P stoichiometry of benthic leaf litter helped to predict stream N:P uptake in temperate deciduous forest streams. These results all suggest that the stoichiometry of benthic biomass may—in some cases—help to predict system-level nutrient demand (also see Webster et al. 2009). Nonetheless, additional research is needed across a broader range of both uptake and benthic stoichiometry to examine this hypothesis.

Our uptake experiments were restricted to NO_3-N and PO_4-P, but similar additions could be conducted with any combination of other nutrients, including other forms of bioavailable N such as ammonium (NH_4^+). Although ammonium concentrations are consistently low or near detection throughout the West Fork watershed (Gardner and McGlynn 2009), uptake of relatively labile NH_4^+ through biotic assimilation or nitrification is likely to be equal to or greater than that of nitrate (e.g., Dortch 1990; Hall and Tank 2003). Thus, studies that aim to examine total dissolved N:P uptake ratios should consider characterizing uptake kinetics of both NH_4^+-N and NO_3-N. In our case, the primary goal was to examine coupling between NO_3-N and PO_4-P using a novel approach.

The value of dual-nutrient uptake surface models

Our dual-nutrient kinetic models allowed us to explore the simultaneous influence of nutrient concentrations *and* stoichiometry on NO_3-N or PO_4-P uptake (Fig. 5). Although multi-substrate approaches have been used in other contexts in efforts to characterize, for example, decomposition of soluble C in soils or

ecoenzymatic activity (e.g., Davidson et al. 2012; Sinsabaugh and Follstad Shah 2012), our study represents one of the first to apply such an approach towards understanding colimitation and uptake kinetics in stream ecosystems. Our M–M model parameters and modeled surfaces showed clear contrasts in uptake patterns among three oligotrophic streams that differed only slightly in abiotic and biotic characteristics.

Coupled nutrient dynamics and network models

Considerable effort has been focused on predicting nutrient uptake and removal across river networks, with the goal of understanding and modeling biogeochemical and hydrologic controls on the transport and fate of anthropogenic nutrients (e.g., Ensign and Doyle 2006; Wollheim et al. 2006; Mulholland et al. 2008). Such efforts are critical for scaling knowledge based on individual experiments and observations to larger river basins (Hall et al. 2013), especially in the context of understanding and mitigating patterns such as large-river eutrophication or hypoxia in the Gulf of Mexico. Yet, most stream network models focus on a single element (typically nitrogen) and do not explicitly incorporate interactions or synergies with other coupled elements. Helton et al. (2011) emphasized the need for parameterizing and testing coupled element network models, which could greatly improve the predictive capabilities of current network models. Our experimental results from three headwater streams demonstrate that failure to incorporate such interactions among nutrients could lead to large deviations between observed and predicted nutrient removal patterns (also see Gibson et al. 2015). Additional empirical work that examines N and P coupling across a range of biotic and abiotic conditions should go far towards informing the construction of coupled element network models in the future.

It is important to note that our experiments were conducted at baseflow within a relatively small time window and at small spatial scales (i.e., August in three streams). In addition, outside of dissolved and epilithic nutrient chemistry, our sites showed little inter-site variation with respect to other environmental characteristics such as light, temperature, and substrate size. We might expect very different patterns of uptake kinetics during other times of the year or in other larger streams where environmental conditions (e.g., light, temperature, flow, geomorphology) and biotic factors (e.g., community structure, biomass) differ. For instance, epilithic biomass and ecosystem metabolism are likely to be positively correlated with measurements of ambient and maximum uptake rates (Hall and Tank 2003). In addition, changes in microbial community structure throughout the year or across space could lead to variation in uptake patters as a result of shifts in nutrient requirements. Efforts to parameterize network models at larger spatiotemporal scales will need to incorporate additional empirical information and/or parameters that account for such differences.

Conclusions

Nutrient cycles are tightly coupled through abiotic and biotic processes, and understanding ecosystem responses to elevated nutrients necessarily requires consideration of multiple, potentially colimiting, elements. In stream ecosystems, the concentrations and stoichiometries of dissolved forms of N and P have shifted drastically as a result of anthropogenic activities that generate excess nutrients, as well as wastewater technologies that remove them (Justic et al. 1995; Dodds 2007; Finlay et al. 2013). Our study represents an important early step in the quest to quantify the *coupling* of N and P uptake at the ecosystem level. This work builds on a rich history of uptake studies in streams (Mulholland and Webster 2010), as well as new and efficient nutrient spiraling methods (Covino et al. 2010a; Trentman et al. 2015). Our approach should be useful for advancing our general understanding of coupled nutrient cycling in streams, as well as providing an empirical toolbox for parameterizing stream network models.

Acknowledgements This research was supported by Montana State University, EPA STAR Grant R832449, EPA 319 funds administered by the Montana Department of Environmental Quality, and the USGS 104(b) grant program administered by the Montana Water Center. Funding was also provided by National Science Foundation EPSCoR program (M66012/66013). We thank Erin Seybold, Kate Henderson, James Hood, and James Junker for colleague reviews and Tim Covino, Kristin Gardner, and Galena Montross for research support and collaboration. We also thank two anonymous

reviewers and Dr. Chris Evans for their very constructive feedback.

Appendix: A series of figures that helps to visualize data resulting from the dual-nutrient additions

This first figure shows concentrations of nitrate-N and phosphate-P during a typical dual-nutrient slug. The bars on the left indicate the mass of each nutrient added during the slug.

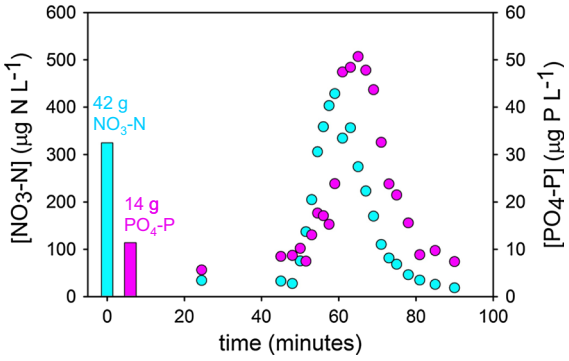

This next figure shows raw data for a typical breakthrough curve for nitrate-N and chloride during a dual slug. Phosphate-P curves look similar, but are offset in time.

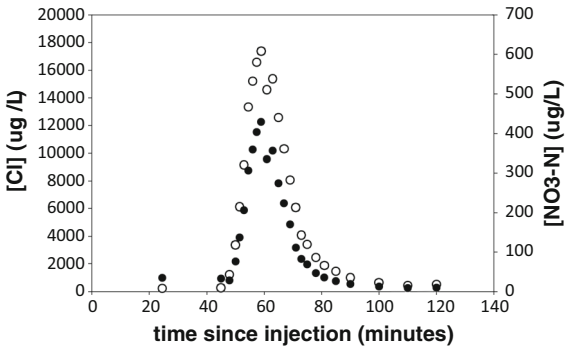

This last figure shows the relationship between observed nitrate concentrations during the slug (y-axis) and expected nitrate concentrations if nitrate was not taken up by stream biota (x-axis). The expected concentration is calculated as the background-corrected chloride concentration multiplied by the ratio of nitrate to chloride in the nutrient slug. The dashed line is a 1:1 line. The difference between this line and the data points represents biological uptake.

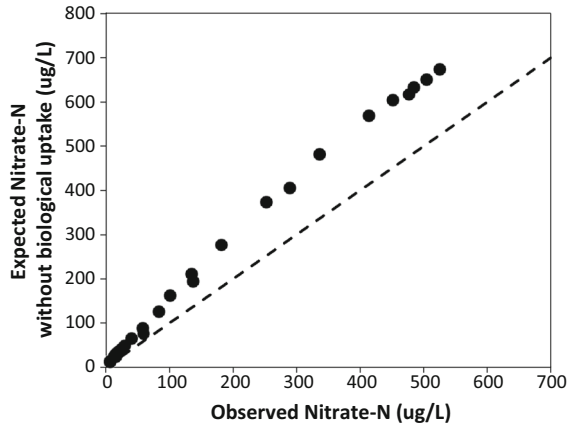

References

Aber JD, Nadelhoffer KJ, Steudler P, Melillo JM (1989) Nitrogen saturation in northern forest ecosystems. BioScience 39:378–386

Allgeier JE, Rosemond AD, Layman CA (2011) The frequency and magnitude of non-additive responses to multiple nutrient enrichment. J Appl Ecol 48:96–101. doi:10.1111/j.1365-2664.2010.01894.x

American Public Health Association (1998) Standard methods for the examination of water and wastewater, 20th edn. American Public Health Association, Washington DC

Appling AP, Heffernan JB (2014) Nutrient limitation and physiology mediate fine-scale (de)coupling of biogeochemical cycles. Am Nat 184:384–406. doi:10.1086/677282

Bernhardt ES, Likens GE, Buso DC, Driscoll CT (2003) In-stream uptake dampens effects of major forest disturbance on watershed nitrogen export. Proc Natl Acad Sci USA 100:10304–10308

Bernot MJ, Dodds WK (2005) Nitrogen retention, removal, and saturation in lotic ecosystems. Ecosystems 8:442–453

Bothwell ML (1989) Phosphorus-limited growth dynamics of lotic periphytic diatom communities: areal biomass and cellular growth rate responses. Can J Fish Aquat Sci 46:1293–1301

Bracken ES, Hillebrand H, Borer ET, Seabloom EW, Cebrian J, Cleland EE, Elser JJ, Gruner DS, Harpole WS, Ngai JT, Smith JE (2015) Signatures of nutrient limitation and co-limitation: responses of autotroph internal nutrient concentrations to nitrogen and phosphorus additions. Oikos 124:113–121

Brookshire ENJ, Valett HM, Thomas SA, Webster JR (2005) Coupled cycling of dissolved organic nitrogen and carbon in a forest stream. Ecology 86:2487–2496

Chapin FS III, Vitousek PM, Cleve KV (1986) The nature of nutrient limitation in plant communities. Am Nat 127:48–58

Cohen MJ, Kurz MJ, Heffernan JB, Martin JB, Douglass RL, Foster CR, Thomas RG (2013) Diel phosphorus variation and the stoichiometry of ecosystem metabolism in a large spring-fed river. Ecol Monogr 83:155–176

Covino TP, McGlynn BL, McNamara RA (2010a) Tracer additions for spiraling curve characterization (TASCC): quantifying stream nutrient uptake kinetics from ambient to saturation. Limnol Oceanogr Methods 8:484–498. doi:10.4319/lom.2010.8.484

Covino TP, McGlynn BL, Baker MA (2010b) Separating physical and biological nutrient retention and quantifying uptake kinetics from ambient to saturation in successive mountain stream reaches. J Geophys Res 115:G04010. doi:10.1029/2009JG001263

Covino TP, McGlynn BL, McNamara RA (2012) Land use/land cover and scale influences on in-stream nitrogen uptake kinetics. J Geophys Res 117:G02006. doi:10.1029/2011JG001874

Cross WF, Benstead JP, Frost PC, Thomas SA (2005) Ecological stoichiometry in freshwater benthic systems: recent progress and perspectives. Freshw Biol 50:1895–1912

Davidson EA, Samanta S, Caramori SS, Savage K (2012) The Dual Arrhenius and Michaelis–Menten kinetics model for decomposition of soil organic matter at hourly to seasonal time scales. Glob Change Biol 18:371–384. doi:10.1111/j.1365-2486.2011.02546.x

Davis JC, Minshall GW (1999) Nitrogen and phosphorus uptake in two Idaho (USA) headwater wilderness streams. Oecologia 119:247–255

Demars BOL (2008) Whole-stream phosphorus cycling: testing methods to assess the effect of saturation of sorption capacity on nutrient uptake length measurements. Water Res 42:2507–2516

Dodds WK (2007) Trophic state, eutrophication and nutrient criteria in streams. Trends Ecol Evol 22:669–676. doi:10.1016/j.tree.2007.07.010

Dodds WK, López AJ, Bowden WB, Gregory S, Grimm NB, Hamilton SK, Hershey AE, Martí E, McDowell WH, Meyer JL, Morrall D, Mulholland PJ, Peterson BJ, Tank JL, Valett HM, Webster JR, Wollheim WM (2002) N uptake as a function of concentration in streams. J N Am Benthol Soc 21:206–220

Dortch Q (1990) The interaction between ammonium and nitrate uptake in phytoplankton. Mar Ecol Prog Ser 61:183–201

Dugdale RC (1967) Nutrient limitation in the sea: dynamics, identification, and significance. Limnol Oceanogr 12:685–695

Earl SR, Valett HM, Webster JR (2006) Nitrogen saturation in stream ecosystems. Ecology 87:3140–3151

Elser JJ, Bracken MES, Cleland EE, Gruner DS, Harpole WS, Hillebrand H, Ngai JT, Seabloom EW, Shurin JB, Smith JE (2007) Global analysis of nitrogen and phosphorus limitation of primary producers in freshwater, marine, and terrestrial ecosystems. Ecol Lett 10:1135–1142

Elser JJ, Kyle M, Steger L, Nydick KR, Baron JS (2009) Nutrient availability and phytoplankton nutrient limitation across a gradient of atmospheric nitrogen deposition. Ecology 90:3062–3073

Ensign SH, Doyle MW (2006) Nutrient spiraling in streams and river networks. J Geophys Res. doi:10.1029/2005JG0001114

Falkowski PG, Fenchel T, Delong EF (2008) The microbial engines that drive Earth's biogeochemical cycles. Science 320:1034–1039. doi:10.1126/science.1153213

Finlay JC, Small GE, Sterner RW (2013) Human influences on nitrogen removal in lakes. Science 342:247–250

Finzi AC, Cole JJ, Doney SC, Holland EA, Jackson RB (2011) Research frontiers in the analysis of coupled biogeochemical cycles. Front Ecol Environ 9:74–80

Francoeur SN (2001) Meta-analysis of lotic nutrient amendment experiments: detecting and quantifying subtle responses. J N Am Benthol Soc 20:358–368

Galloway JN, Townsend AR, Erisman JW, Bekunda M, Cai Z, Freney JR, Martinelli LA, Seitzinger SP, Sutton MA (2008) Transformation of the nitrogen cycle: recent trends, questions, and potential solutions. Science 320:889–892

Gardner KK, McGlynn BL (2009) Seasonality in spatial variability and influence of land use/land cover and watershed characteristics on streamwater nitrate concentrations in a developing watershed in the Rocky Mountain west. Water Resour Res 45:W08411. doi:10.1029/2008WR007029

Gardner KK, McGlynn BL, Marshall L (2011) Quantifying watershed sensitivity to spatially variable N loading and the relative importance of watershed N retention mechanisms. Water Resour Res 47:W08524. doi:10.1029/2010WR009738

Gibson CA, O'Reilly CM (2012) Organic matter stoichiometry influences nitrogen and phosphorus uptake in a headwater stream. Freshw Sci 31:395–407

Gibson CA, O'Reilly CM, Conine AL, Lipshutz SM (2015) Nutrient uptake dynamics across a gradient of nutrient concentrations and ratios at the landscape scale. J Geophys Res. doi:10.1002/2014.JG002747

Hall RO Jr, Tank JL (2003) Ecosystem metabolism controls nitrogen uptake in streams in Grand Teton National Park, Wyoming. Limnol Oceanogr 48:1120–1128

Hall RO Jr, Baker MA, Rosi-Marshall EJ, Tank JL, Newbold JD (2013) Solute-specific scaling of inorganic nitrogen and phosphorus uptake in streams. Biogeosciences 10:7323–7331. doi:10.5194/bg-10-7323-2013

Hansen AJ, Rasker R, Maxwell B, Rotella JJ, Johnson JD, Parmenter AW, Langner U, Cohen WB, Lawrence RL, Kraska MPV (2002) Ecological causes and consequences of demographic changes in the new west. BioScience 52:151–162

Harpole WS, Ngai JT, Cleland EE, Seabloom EW, Borer ET, Bracken MES, Elser JJ, Gruner DS, Hillebrand H, Shurin JB, Smith JE (2011) Nutrient co-limitation of primary producer communities. Ecol Lett 14:852–862

Helton AM, Poole GC, Meyer JL, Wollheim WM, Peterson BJ, Mulholland PJ, Bernhardt ES, Stanford JA, Arango C, Ashkenas LR, Cooper LW, Dodds WK, Gregory SV, Hall RO Jr, Hamilton SK, Johnson SL, McDowell WH, Potter JD, Tank JL, Thomas SM, Valett HM, Webster JR, Zeglin L (2011) Thinking outside the channel: modeling nitrogen cycling in networked river ecosystems. Front Ecol Environ 9:229–238. doi:10.1890/080211

Howarth RW (1988) Nutrient limitation of net primary production in marine ecosystems. Annu Rev Ecol 19:89–110

Johnson LT, Tank JL, Arango CP (2009) The effect of land use on dissolved organic carbon and nitrogen uptake in streams. Freshw Biol 54:2335–2350

Justić D, Rabalais NN, Turner RE (1995) Stoichiometric nutrient balance and origin of coastal eutrophication. Mar Pollut Bull 30:41–46

King SA, Heffernan JB, Cohen MJ (2014) Nutrient flux, uptake, and autotrophic limitation in streams and rivers. Freshw Sci 33:85–98. doi:10.1086/674383

Lewis WM Jr, Wurtsabugh WA (2008) Control of lacustrine phytoplankton by nutrients: erosion of the phosphorus paradigm. Int Rev Hydrobiol 93:446–465

Lohman K, Jones JR, Baysinger-Daniel C (1991) Experimental evidence for nitrogen limitation in a northern Ozark stream. J N Am Benthol Soc 10:14–23

Marklein AR, Houlton BZ (2012) Nitrogen inputs accelerate phosphorus cycling rates across a wide variety of terrestrial ecosystems. New Phytol 193:696–704

Martí E, Fonollà P, von Schiller D, Sabater F, Argerich A, Ribot M, Riera JL (2009) Variation in stream C, N and P uptake along an altitudinal gradient: a space-for-time analogue to assess potential impacts of climate change. Hydrol Res 40:123–137

Megee RD, Drake JF, Fredrickson AG, Tsuchiya HM (1972) Studies in intermicrobial symbiosis, *Saccharomyces cerevisiae* and *Lactobacillus casei*. Can J Microbiol 18:1733–1742

Melillo JM, Field CB, Moldan B (eds) (2003) Interactions of the major biogeochemical cycles: global change and human impacts. Island Press, Washington, DC

Monod J (1950) La technique de culture continue; théorie et applications. Ann I Pasteur Paris 79:390–410

Montross G, McGlynn BL, Montross S, Gardner K (2013) Nitrogen production from geochemical weathering of rocks in southwest Montana, USA. J Geophys Res. doi:10.1002/jgrg.20085

Mulholland PJ, Webster JR (2010) Nutrient dynamics in streams and the role of *J-NABS*. J N Am Benthol Soc 29:100–117

Mulholland PJ, Tank JL, Webster JR, Bowden WB, Dodds WK, Gregory SV, Grimm NB, Hamilton SK, Johnson SL, Martí E, McDowell WH, Merriam JL, Meyer JL, Peterson BJ, Valett HM, Wollheim WM (2002) Can uptake length in streams be determined by nutrient addition experiments? Results from an interbiome comparison study. J N Am Benthol Soc 21:544–560

Mulholland PJ, Helton AM, Poole GC, Hall RO Jr, Hamilton SK, Peterson BJ, Tank JL, Ashkenas LR, Cooper LW, Dahm CN, Dodds WK, Findlay SEG, Gregory SV, Grimm NB, Johnson SL, McDowell WH, Meyer JL, Valett HM, Webster JR, Arango CP, Beaulieu JJ, Bernot MJ, Potter JD, Sheibley RW, Sobota DJ, Thomas SM (2008) Stream denitrification across biomes and its response to anthropogenic nitrate loading. Nature 452:202–206. doi:10.1038/nature06686

O'Brien JM, Dodds WK (2010) Saturation of NO_3^- uptake in prairie streams as a function of acute and chronic N exposure. J N Am Benthol Soc 29:627–635

O'Brien JM, Dodds WK, Wilson KC, Murdock JN, Eichmiller J (2007) The saturation of N cycling in Central Plains streams: ^{15}N experiments across a broad gradient of nitrate concentrations. Biogeochemistry 84:31–49

Payn RA, Webster JR, Mulholland PJ, Valett HM, Dodds WK (2005) Estimation of stream nutrient uptake from nutrient addition experiments. Limnol Oceanogr Methods 3:174–182

Powers SM, Stanley EH, Lottig NR (2009) Quantifying phosphorus uptake using pulse and stead-state approaches in streams. Limnol Oceanogr Methods 7:498–508

Reddy KR, Kadlec RH, Flaid E, Gale PM (1999) Phosphorus retention in streams and wetlands: a review. Crit Rev Environ Sci Technol 29:83–146. doi:10.1080/10643389991259182

Rier ST, Kinek KC, Hay SE, Francoeur SN (2016) Polyphosphate plays a vital role in the phosphorus dynamics of stream periphyton. Freshw Sci 35:490–502. doi:10.1086/685859

Rodríguez-Cardona B, Wymore AS, McDowell WH (2015) DOC:NO_3^- ratios and NO_3^- uptake in forested headwater streams. J Geophys Res. doi:10.1002/2015JG003146

Schade JD, MacNeill K, Thomas SA, McNeely FC, Welter JR, Hood JM, Goodrich M, Power ME, Finlay JC (2011) The stoichiometry of nitrogen and phosphorus spiraling in heterotrophic and autotrophic streams. Freshw Biol 56:424–436

Schlesinger WH, Cole JJ, Finzi AC, Holland EA (2011) Introduction to coupled biogeochemical cycles. Front Ecol Environ 9:5–8

Simon KS, Townsend CR, Biggs JF, Bowden WB (2005) Temporal variation of N and P uptake in 2 New Zealand streams. J N Am Benthol Soc 24:1–18

Sinsabaugh RL, Follstad Shah JJ (2012) Ecoenzymatic stoichiometry and ecological theory. Annu Rev Ecol Evol Syst 43:313–343. doi:10.1146/annurev-ecolsys-071112-124414

Steinman AD, Lamberti GA, Leavitt PR (2006) Biomass and pigments of benthic algae. In: Hauer FR, Lamberti GA (eds) Methods in stream ecology. Academic Press, Burlington, pp 367–379

Sterner RW (2008) On the phosphorus limitation paradigm for lakes. Int Rev Hydrobiol 93:433–445

Sterner RW, Hessen DO (1994) Algal nutrient limitation and the nutrition of aquatic herbivores. Annu Rev Ecol Syst 25:1–29

Sterner RW, Elser JJ (2002) Ecological stoichiometry. Princeton University Press, Princeton

Stream Solute Workshop (1990) Concepts and methods for assessing solute dynamics in stream ecosystems. J N Am Benthol Soc 9:95–119

Trentman MT, Dodds WK, Fencl JS, Gerber K, Guarneri J, Hitchman SH, Peterson Z, Rüegg J (2015) Quantifying ambient nitrogen uptake and functional relationships of uptake versus concentration in streams: a comparison of stable isotope, pulse, and plateau approaches. Biogeochemistry 125:65–79. doi:10.1007/s10533-015-0112-5

Webster JR, Valett HM (2007) Solute dynamics. In: Hauer FR, Lamberti GA (eds) Methods in stream ecology. Academic Press, San Diego, pp 169–185

Webster JR, Newbold JD, Thomas SA, Valett HM, Mulholland PJ (2009) Nutrient uptake and mineralization during leaf decay in streams—a model simulation. Int Rev Hydrobiol 94:372–390

Wollheim WM, Vörösmarty CJ, Peterson BJ, Seitzinger SP, Hopkinson CS (2006) Relationship between river size and nutrient removal. Geophys Res Lett 33:L06410. doi:10.1029/2006GL025845